Nanoscale

Accepted Manuscript

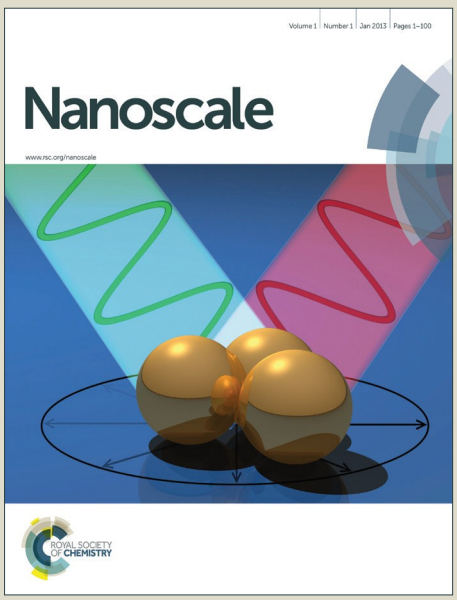

ROYAL SOCIETY OF CHEMISTRY

www.rsc.org/nanoscale

A Miniaturized Microbial Fuel Cell with Three-Dimensional Graphene Macroporous Scaffold Anode Demonstrating a Record Power Density of Over 10,000 Wm^{-3}

Hao Ren[1, *], He Tian[2, #], Cameron L. Gardner[3, †], Tian-Ling Ren[2] and Junseok Chae[1]
[1] Hao Ren, Prof. Junseok Chae
School of Electrical, Computer and Energy Engineering, Arizona State University, Tempe, AZ 85287 (USA)
[*]E-mail: hren12@asu.edu
[2] Tian He, Prof. Tian-Ling Ren
Institute of Microelectronics & Tsinghua National Laboratory for Information Science and Technology (TNList), Tsinghua University, Beijing, 10084 (P. R. China)
[#]Current Address: Ming Hsieh Department of Electrical Engineering, University of Southern California, Los Angeles, CA 90089 (USA)
[3] Cameron L. Gardner
School of Biological and Health Systems Engineering, Arizona State University, Tempe, AZ 85287 (USA)
[†]Current Address: Department of Genetics, Harvard Medical School, Boston, MA 02115 (USA)

Abstract: A microbial fuel cell (MFC) is a bio-inspired renewable energy converter which directly converts biomass into electricity. This is accomplished via the unique extracellular electron transfer (EET) of a specific species of microbe called the exoelectrogen. Many studies have attempted to improve the power density of MFCs, yet the reported power density is still nearly two orders of magnitude lower than other power sources/converters. Such low performance can primarily be attributed to two bottlenecks: i) ineffective electron transfer from microbes located far from the anode and ii) an insufficient buffer supply to the biofilm. This work takes a novel approach to mitigate these two bottlenecks by integrating a three-dimensional (3D) macroporous graphene scaffold anode in a miniaturized MFC. This implementation has delivered the highest power density reported of over 10,000 Wm^{-3} in all MFCs to date. The miniaturized configuration offers a high surface area to volume ratio and improved mass transfer of biomass and buffers. The 3D graphene macroporous scaffold warrants investigation due to its high specific surface area, high porosity, and excellent conductivity and biocompatibility which

facilitates EET and alleviates acidification in the biofilm. Consequently, the 3D scaffold houses an extremely thick and dense biofilm from *Geobacter*-enriched culture, delivering an areal/volumetric current density of 15.51 Am^{-2} / 31,040 Am^{-3} and a power density of 5.61 Wm^{-2} / 11,220 Wm^{-3}, a 3.3 fold increase when compared to the planar 2D control counterparts.

Keywords: Microbial fuel cell; Three-dimensional graphene; Miniaturization; Bio-inspired devices; Power density;

A surplus of harvestable, green, and renewable energy exists and is stored in biomass. This energy source has the potential to offset world-wide concerns regarding global warming and energy depletion. Biomass is the largest renewable energy source in use to date, accounting for approximately 10% (50 EJ, 5×10^{19} J) of world total primary energy source[1]. This is equivalent to a power of 1.59 TW, or 64.5% of total world-wide electricity net generation (77.5 EJ) in 2012[2]. While such an energy source exists, most of the requisite biomass is consumed in a highly inefficient manner through use in heating and cooking with open fires. Additionally, such a utilization manner has considerable deleterious impacts on general health and on the environment. Many studies are seeking new ways to capture and convert this major source of green renewable energy into high efficiency fuel or electricity[3-6].

A microbial fuel cell (MFC) is an electrochemical fuel cell that directly converts the chemical energy of organic compounds from biomass to electrical energy[5, 7-9]. This is accomplished via catalytic reactions of specific microbes called exoelectrogens, or anode respiring bacteria[10]. MFCs are particularly attractive when compared to traditional biomass utility technologies such as incineration and gasification, primarily due to the direct highly efficient electricity conversion.

Many different microbe communities have been discovered which can reduce various organic substances such as wastewater, marine sediment, inorganic waste, and even nuclear waste[11]. The catalytic living microbes in MFCs regenerate themselves, which allows for higher efficiency when compared to enzymatic fuel cells which require continuous supplementation of an external catalyst[11].

To date, the highest power reported for an MFC is 3,320 Wm^{-3}, which is several to hundreds of folds lower than conventional power sources/converters such as lithium ion batteries and hydrogen fuel cells[12]. Many studies have sought to enhance catalytic activity and improve the overall performance of MFCs. For example, researchers have investigated improving performance by reducing electrode resistance, improving mass transfer of organic compounds / H^+ carrying buffers, implementing materials with properties of high surface area to volume ratios / high electrical conductivities, and improving the configuration of MFCs[13].

Miniaturized power sources/converters have become an active area of research, focusing specifically on devices such as piezoelectric nanogenerators[14], ultra-fast charge-discharge batteries[15], and ultra-high-power micrometer-sized supercapacitors[16]. These devices benefit from a small footprint, a high surface area to volume ratio, and a short charging time. Furthermore, the miniaturized power sources/converters often benefit from micro/nano-fabrication and batch manufacturing, resulting in precisely-controlled geometries, small variances among devices, and low cost[13]. Similar attempts have been taken for MFCs[13, 17-21]. Micro-scale MFCs originally reported a volumetric power of 0.3 - 4.2 Wm^{-3} which is more than 200 times lower than that of macro/meso-scale counterparts when micro-scale MFCs were at an early stage of development[22, 23]. Over the past seven years, however, the volumetric power density of micro-scale MFCs has been enhanced by almost three orders of magnitudes and has surpassed that of macro/meso-scale

MFCs[17, 24]. This significant improvement is a derivative of the benefits of a small characteristic length for configuration which offers a high surface area to volume ratio and improved mass transfer of organic compounds / H^+ carrying buffers[18]. Similar attempts to adopt a small characteristic length have been incorporated into macro/meso-scale MFCs which has recapitulated this dramatic increase in power density leading to the highest volumetric power densities in macro/meso-scale MFCs to date[24, 25].

While many different materials have been adopted as electrodes, carbon based materials have been implemented as electrodes due to their ease of access, low expense, decent conductivity, and stability[11, 26-30]. More recently, nanostructured carbon-based materials have become widely used as the anode, either in planar or in 3-dimensional (3D) form, due to their further magnified electrical conductivity, high surface area to volume ratio, mechanical/thermal stability, and low cost. Planar electrodes incorporate carbon-based nanostructured materials, such as carbon nanotubes (CNT) and graphene on top of a planar surface where the exoelectrogens form a biofilm[17, 31]. Such constructs have shown areal / volumetric power densities of 0.83 Wm^{-2} / 3,320 Wm^{-3} based on the projected anode area and anode chamber volume. 3D electrodes are attractive as they allow for the growth of a thicker exoelectrogen biofilm. According to prior studies on the electron transfer of biofilms, the exoelectrogens located tens of micrometers away from the anode have difficulty transferring electrons to the anode due to extracellular electron transfer (EET) limitations[32-35]. A variety of 3D nanostructured carbon-based electrodes have been adopted in MFCs including CNT textiles[36], conductive polypyrrole (PPy)/reduced graphene oxide[37], chitosan/vacuum-stripped graphene scaffold[38], reduced graphene oxide/CNT coated scaffold[39, 40], polyaniline hybridized graphene[41], reduced graphene oxide on carbon fiber[42], CNT/polyaniline or CNT/chitosan composite[43, 44], reduced graphene oxide on sponges[45], and 3D

graphene on Ni foam[40, 46]. Such 3D nanostructured carbon-based electrode constructs feature a high effective surface area and conductivity and deliver maximum areal/volumetric power densities of 1.57 Wm^{-2} and 394 Wm^{-3} respectively.

Prior work has reported specific factors for the hampering of catalytic activities of exoelectrogens. Primary hampering effects are due to ineffective electron transfer of microbes located far from the anode and insufficient buffer supply to the bacterial biofilm. Malvankar *et al.* reported that the low conductivity of the biofilm limited the current density of *Geobacter sulfurreducens*[32]. Liu *et al.* found that reduced *cytochrome c* accumulated in thick biofilms, suggesting that *cytochrome c* located far from the anode has a limited capability to transfer electrons to the anode[34]. Torres *et al.* reported that ineffective proton transport and resultant acidification inside the biofilm caused current density to drop significantly[47]. Franks *et al.* further corroborated this acidification effect in another study and reported that the pH of the biofilm close to the anode was as low as 6.1, which significantly limits the metabolism and current density of *Geobacter sulfurreducens*[48].

In this study, we analyze and compare the effects of 3D graphene macroporous scaffold anodes on the current and power densities of miniaturized MFCs with those of planar 2D counterparts, in an attempt to mitigate the aforementioned catalytic hampering phenomena. The 3D graphene scaffold is embedded in a 50 μL miniaturized reactor to form a highly populated dense biofilm from *Geobacter*-enriched mixed bacterial culture, which is then characterized in its biofilm morphology, polarization curves, and current / power densities. The planar 2D counterparts, including single layer graphene and a control current collector (CC), are evaluated side by side. This comprehensive comparative study offers the unique opportunity to evaluate the impact of 3D constructs on the power density of MFCs.

Results and Discussions

Miniaturized MFCs with 2D and 3D Graphene Based Anodes

Fig. 1(a) shows a schematic of a miniaturized MFC having 1 cm^2 graphene-based anode variants, including 2D single layer graphene and a 3D graphene scaffold. The scanning electron microscopy (SEM) images of corresponding anodes are illustrated in Fig. 1(b, d). 3D graphene scaffolds are spaced by approximately 100-200 μm. This spacing provides efficient mass transfer to facilitate EET. Fig. 1(c) shows the typical Raman spectra of 3D graphene scaffold. There are two sharp peaks, a 2D-band peak at ~2697 cm^{-1} and a G-band peak at ~1581 cm^{-1}. The 2D to G ratio is 0.18, indicating that it is few-layer graphene, which is in agreement with previous reported Raman of 3D graphene scaffold[49]. Fig. S-1 illustrates the Raman spectra of the single layer graphene. Typical G and 2D peak are observed, indicating the single-layer graphene.

Biofilm Formation on 2D and 3D Graphene Anodes

Assembly of the MFCs with variant anodes are shown in Fig. S-2. The MFCs with variant anodes were all successfully started up in 7-14 days and Fig. S-3 shows the start-up process of current density versus time. Biofilms on 2D and 3D graphene anodes were visualized to characterize the morphology of their respective biofilms. The SEM and optical profilometer images after biofilm growth, as shown in Fig. 2(a, b), demonstrate thick and dense biofilm formation. This thickness of 150-200 μm and density of 1.6×10^{11} *Geobacter sulfurreducens* / cm^2 (calculated based on equation S-1), formed on the 3D graphene scaffold generated the highest current and power density reported. The biofilm thickness is comprised of 5-6 stacks of graphene scaffolds. The single layer graphene (Fig. 2(c, d)) yielded a thick biofilm of ~ 20-40 μm - equivalent to a density of 2.8×10^{10} *Geobacter sulfurreducens* / cm^2 - which is consistent with the highest current and power density recorded among planar 2D anodes. The biofilm on the

control was thin, at ~ 2-3 μm, 2.3×10^9 *Geobacter sulfurreducens* / cm^2 (Fig. 2(e, f)), only a few layers of exoelectrogen were present yielding correspondingly low current and power densities.

Current and Power Density of Miniaturized MFCs

Fig. 3 shows the polarization curves of miniaturized MFCs with variant electrodes. The control showed a low sheet resistance of 3.65 Ω/square, and delivered a maximum current density of 2.20 ± 0.01 Am^{-2} / $8,800 \pm 40$ Am^{-3} with a power density of 0.84 ± 0.01 Wm^{-2} / $3,360 \pm 40$ Wm^{-3}. The 2D single layer graphene was fabricated by chemical vapor deposition (CVD) and showed sheet resistance of 4.13 Ω/square, current density of 6.06 ± 0.05 Am^{-2} / $24,240 \pm 200$ Am^{-3} and power density of 2.46 ± 0.04 Wm^{-2}/ $8,840 \pm 160$ Wm^{-3}, a 1.75 and 1.96 fold improvement respectively over those of the control. The high performance of the 2D single layer graphene is believed to be due to excellent conductivity, biocompatibility, and electrochemical characteristics of the 2D graphene[50] which results in thicker and denser biofilm formation as illustrated by the SEM and optical profilometry results.

The 3D graphene scaffold was fabricated by chemical vapor deposition (CVD) on a nickel foam template, which was subsequently etched to form a free-standing 3D macroporous graphene scaffold. The fabrication process of the graphene based electrodes are detailed in electronic supplementary information (ESI). This fabrication strategy is a low-cost approach to construct 3D graphene with a high surface area to volume ratio[49]. The 3D graphene macroporous scaffold was spaced by approximately 100-200 μm and showed very low sheet resistance at 0.335 Ω/square. The 3D graphene macroporous scaffold addresses two of the stubborn bottlenecks comprised of the reduction of electron transfer efficiency of microbes located far from the anode, and insufficient buffer supply to the bacterial biofilm which have impeded MFCs in their ability to achieve high power density. The 3D scaffold provides high specific surface area, high porosity,

excellent conductivity, and biocompatibility. All of these features offer a spacious and optimized environment for the exoelectrogen to form a thick and dense biofilm. Specifically, the excellent conductivity mitigates the ineffective electron transfer of microbes far from the anode, and the high porosity mitigates the insufficient buffer supply to the bacterial biofilm. This biofilm demonstrated substantial current and power density improvements over its 2D counterparts. Maximum current and power densities of 10.23 Am^{-2} ± 0.46 Am^{-2} / 20,460 Am^{-3} ± 920 Am^{-2} and 3.86 ± 0.02 Wm^{-2} / 7,720 ± 40 Wm^{-3} were obtained at a flow rate of 18 µL/min. As the flow rate increased to 32 µL/min, the miniaturized MFC delivered maximum current and power densities of 15.51 ± 0.30 Am^{-2} / 31,020 ± 600 Am^{-3} and 5.61 ± 0.35 Wm^{-2} / 11,220 ± 700 Wm^{-3}, which corresponds to a more than 3.3 fold improvement when compared to the control. The volumetric power density of 11,220 Wm^{-3} reported here is the highest power density reported and is over 28.5 fold that of 3D nanostructured carbon-based electrodes[19].

Internal Resistance and Current/Power Density of Miniaturized MFCs Having Planar 2D and 3D Anodes

The internal resistance of MFCs significantly impacts current and power generation. The maximum areal current and power densities of an MFC are defined as[13]:

$$i_{\max,areal} = \frac{I_{\max}}{A} = \frac{E_{OCV}}{R_i \cdot A}$$

$$p_{\max,areal} = \frac{P_{\max}}{A} = \frac{{E_{OCV}}^2}{4R_i \cdot A} \quad (1)$$

where $i_{max,\ areal,}$ $p_{max,\ areal}$, I_{max}, P_{max}, E_{ocv}, R_i, *and* A are the maximum areal current density, maximum areal power density, maximum current, maximum power, open circuit voltage, internal resistance, and electrode projected area, respectively. At a given configuration of an

MFC, both E_{OCV} and A are constants, so as the internal resistance decreases, the maximum areal and volumetric current/power densities increase.

Internal resistances of the MFC with differing anodes were calculated by linearly fitting the ohmic region of the polarization curves in Fig. 3(a), as compiled in Table 1. Areal resistivity is internal resistance normalized to the anode area of 1 cm^2. The lowest internal resistance/areal resistivity of 219 ± 10 Ω / 219 ± 10 Ω·cm^2 is obtained by the 3D graphene scaffold. The single layer graphene and the control show relatively high internal resistance/areal resistivities, which are 2.2 and 7.4 fold that of the 3D graphene, respectively. The areal resistivity of the 3D graphene anode is at least 4 fold lower than in previously reported carbon-based anode MFCs[17].

The internal resistance of the MFC can be subdivided by the following expression:

$$R_i = R_a + R_c + R_m + R_e \quad (2)$$

where R_i is the total internal resistance and R_a, R_c, R_m, R_e are the ohmic resistance of the anode, cathode, ion exchange membrane, and anolyte/catholyte, respectively. R_a is comprised of the ohmic resistance of the anode which includes the equivalent ohmic resistance of electron generation/transfer from the exoelectrogen to the anode. R_a is a function of the electrical conductivity of the anode, the population of exoelectrogen, the mechanism of electron transfer from exoelectrogen to anode, the acidification inside the biofilm, as well as many other factors[17, 21]. R_c involves the ohmic resistance of the cathode, including the equivalent charge transfer resistance of reducing ions at the cathode. R_m is determined by the equivalent ohmic resistance of the proton exchange membrane. R_e is a function of the distance between the anode and cathode as well as the specific conductivity of the electrolyte. Prior studies report that R_e, R_m, and R_c are all low, on the order of 10 Ω or sub-10 Ω range[17]. Therefore R_a, the anode resistance, dominates

the internal resistance. The anode resistance is believed to arise from the limited catalytic capability of the biofilm on the anode.

Catalytic reactions at the anode limit the power density of MFCs regardless of the planar 2D or 3D electrode configuration. The 2D graphene marks a lower internal resistance and higher current/power generation capability, suggesting that graphene has better electrochemical characteristics and biocompatibility when compared to the control. The 3D scaffold anode shows significantly lower internal resistance and higher current/power density over 2D counterparts. This agrees with prior studies on the rate-limiting step of the EET of exoelectrogens[33, 34, 51]. As the biofilm grows, the catalytic reactions of the biofilm become ineffective for current generation due to two contributing factors: i) limited EET of exoelectrogens far from the anode and ii) an acidification effect derived from exoelectrogen proximity to the anode resulting in insufficient H^+ carrying buffer[33, 48, 52]. 3D porous electrodes address these two challenges by including conductive grids. These grids are spaced by approximately 100-200 μm to minimize the ineffective EET of microbes located far from anode and potentially alleviate acidification inside the biofilm, which is supported by a uni-directional mass transfer model and experimental results, as detailed in ESI. The two effects of facilitating EET and alleviating acidification yield substantially higher current / power densities when compared to planar 2D electrodes.

Besides the two effects, minimizing oxygen intrusion is also essential for achieving a high power density of the *Geobacter*-enriched MFC. Unlike another commonly-adopted microbe, *Shewanella oneidensis* MR-1, *Geobacter sulfurreducens* demands oxygen-free environment to effectively harvest electrons. In macro-/meso-scale settings creating oxygen-free environment may not be a big challenge, however it is often very difficult to achieve oxygen-free environment in micro-scale devices. Many prior miniaturized MFCs used Polydimethylsiloxane (PDMS) as

the building material, which has a rather high oxygen permeability (52,531 ± 1,313 cm^3 $mm/m^2/day/atm$)[13]. In a previous work by our group, Choi *et al.* 2011, we added *L-cysteine* into the anolyte to observe the impact of oxygen on the current/power density of *Geobacter sulfurreducens* based MFC[21]. The result suggested removing oxygen in the anode chamber becomes very effective to enhance current / power density. Since then, we replaced PDMS with glass, which has little oxygen permeability to minimize the oxygen intrusion for the formation of an optimized biofilm. The 3D graphene macroporous scaffold anode MFC was characterized for its coulombic efficiency (CE) to verify the mitigation in oxygen intrusion, by following the experimental procedure in ESI. The MFC marked a high CE of 83% (Fig. S-8), which suggests the successful mitigation of oxygen intrusion, when compared to 31% CE in previous work[21].

Table 2 lists a comparison of performance specifications of this work with prior art. Both the volumetric current and power densities are the highest among all MFCs, regardless of scale[19-21, 23, 53, 54]. The areal/volumetric current and power densities are 5.99/2.99 and 6.76/3.83 fold higher than previously reported miniaturized MFCs, respectively. These high current and power densities are attributed to the excellent biocompatibility characteristics of graphene and the high specific surface area of the 3D graphene scaffold structure.

Potential of *Geobacter Sulfurreducens* based MFCs

Jiang *et al.* predicted a maximum current density of 10^6 Am^{-3} for *Geobacter sulfurreducens*[55]. This extrapolated prediction was calculated from the measured current of a single *Geobacter sulfurreducens* cell. Our record of 3.1×10^4 Am^{-3} is merely 3.1% of the predicted maximum current density, leaving plenty of room for improvement. A number of different approaches to

further improve the current density exist and include implementing sophisticated nanomaterial-based electrodes and genetically engineering exoelectrogens[56, 57].

When compared to other types of both renewable and non-renewable power sources/converters, as illustrated in Fig. 4, the volumetric power density of the MFC with a 3D graphene scaffold is one to three orders of magnitude higher than thermoelectricity (TE), piezoelectricity (PE), indoor photovoltaics (indoor PV), and commercially available lithium manganese dioxide batteries (Sony CR1620[12, 58]), and is comparable to commercially available outdoor photovoltaics (outdoor PV), lead-acid batteries, nickel-cadmium (Ni-Cd) batteries, and lithium ion batteries[12]. The miniaturized MFC may find potential applications to supply power for low power electronics including sub-1mW low power microcontroller units (MCU), neural signal acquisition systems, wireless sensor networks, and implantable medical devices. Miniaturized MFCs also continue to show increasing potential within space exploration for power supply and waste treatment[59-63]. Several studies have reported higher power demands being met by stacking individual MFCs, indeed many of the technical challenges associated with stacking have been effectively addressed[64, 65]. The miniaturized MFCs may take a similar approach, being stacked in series and parallel to increase voltage and current readouts to enhance output power.

Conclusion

This study reports a miniaturized MFC with a 3D graphene scaffold capable of accommodating a high population of microbes. A thick biofilm of 150-200 μm with a density of 1.6×10^{11} *Geobacter sulfurreducens* / cm^2 was obtained due to the high conductivity, high specific area, and high porosity of the 3D graphene scaffold. These structural benefits are believed to facilitate EET and alleviate acidification in the biofilm. Consequently, the highest power density to date of

11,220 Wm^{-3} has been recorded, a more than 3 fold increase over the highest value reported in all previous studies. The high volumetric power density is comparable with commercially available power sources, such as lead-acid batteries, nickel-cadmium batteries, and lithium ion batteries, which makes it a promising candidate as a carbon-neutral, renewable power source.

Experimental

MFC setup and operation

Fabrication and assembly procedures of the anodes and MFCs are detailed in the electronic supplementary information (ESI). The inoculum for the miniaturized MFC was obtained from an acetate-fed microbial electrolysis cell (MEC) that had been continuously operated for more than 6 months and had a *Geobacter*-enriched bacterial community originally from anaerobic-digestion sludge. The anolyte was composed of a 25-mM sodium acetate medium (pH 7.8 ± 0.2). The inoculum and anolyte were mixed at a volumetric ratio of 1:1 for the start-up process. The catholyte was composed of 50-mM potassium ferricyanide in a 100-mM phosphate buffer solution (pH 7.4). The anolyte and catholyte were fed into the miniaturized MFC using a syringe pump (Harvard Instrument Inc.). Prior to being supplied to the MFCs, both anolyte and catholyte were purged with nitrogen for 30 minutes. The MFCs operated at 40 ± 3°C. For each type of anode, at least three identical MFCs were successfully built and characterized.

Data acquisition

The current generated by the MFCs was recorded every minute by measuring the voltage drop across an external resistor connected between the anode and the cathode using a data acquisition system (DAQ/68, National Instrument) with a customized Labview Interface. During start-up, the MFCs were operated at 0.25-2 μL/min and the external resistor was set to 148-Ω. Once the

start-up process completed, the flow rate was increased until the maximum current and power densities were obtained and a polarization measurement was performed. For the polarization curve measurement, a series of resistors were employed, ranging from 148-Ω to 1 MΩ and open circuit.

Calculation and Analysis

The current through the resistor was calculated via Ohm's law ($I = V/R$), where V is the voltage measured across resistor. MFC output power was calculated via Joule's law ($P = I^2R$). Areal and volumetric current/power density were calculated by $I_{areal} = I/A$, $P_{areal} = P/A$ and $I_{volumetric} = I/V$, $P_{volumetric} = P/V$, where A and V were the projected anode area and the anode chamber volume. Polarization curves were plotted according to the voltage output and current / power densities. Internal resistance (R_i) was obtained by linearly fitting the ohmic region of the polarization curve. Areal resistivity was obtained by the equation $r_i = R_i \cdot A$.

SEM and Optical Profilometer Imaging

The anodes were disassembled and rinsed in phosphate buffer saline (PBS). Adherent exoelectrogen cells on the anodes were fixed in a 2% glutaraldehyde solution for 24 hours at 4 °C (Glutaraldehyde solution, Grade I, 25% in H_2O, Sigma Aldrich). Samples were then dehydrated by serial 10 minute transfers through 50, 70, 90, and 100% ethanol. A thin gold film with a thickness of ~10 nm was deposited onto the sample by magnetic sputtering to improve conductivity for SEM imaging. Biofilms on anodes were then examined using field emission scanning electron microscopy (FESEM) (Hitachi S-4700-II) or an environmental SEM (XL30 ESEM-FEG). The anodes before biofilm growth were imaged using an environmental SEM (XL30 ESEM-FEG). The optical profilometer images are taken by a Zygo Zescope optical profiling system (Zygo Corporation).

Acknowledgements

This work was supported by National Natural Science Foundation (61025021, 61434001), 973 Program (2015CB352100), National Key Project of Science and Technology (2011ZX02403-002) and Special Fund for Agroscientific Research in the Public Interest (201303107) of China.

References

1. Medium-Term Renewable Energy Market Report, 2014. ISBN 978-92-64-21821-52.
2. International Energy Statistics - Electricity, DOE/EIA-0383(2012); U.S. Energy Information Administration (EIA): Washington, DC, 2012.
3. J. A. Turner, *Science*, 1999, **285**, 687-689.
4. A. J. Ragauskas, C. K. Williams, B. H. Davison, G. Britovsek, J. Cairney, C. A. Eckert, W. J. Frederick, J. P. Hallett, D. J. Leak and C. L. Liotta, *Science*, 2006, **311**, 484-489.
5. B. E. Logan and K. Rabaey, *Science*, 2012, **337**, 686-690.
6. M. E. Himmel, S.-Y. Ding, D. K. Johnson, W. S. Adney, M. R. Nimlos, J. W. Brady and T. D. Foust, *Science*, 2007, **315**, 804-807.
7. P. L. McCarty, J. Bae and J. Kim, *Environmental science & technology*, 2011, **45**, 7100-7106.
8. B. E. Logan, *Environmental science & technology*, 2004, **38**, 160A-167A.
9. R. D. Perlack, L. L. Wright, A. F. Turhollow, R. L. Graham, B. J. Stokes and D. C. Erbach, *Biomass as feedstock for a bioenergy and bioproducts industry: the technical feasibility of a billion-ton annual supply*, DTIC Document, 2005.
10. B. E. Logan, B. Hamelers, R. Rozendal, U. Schröder, J. Keller, S. Freguia, P. Aelterman, W. Verstraete and K. Rabaey, *Environmental Science & Technology*, 2006, **40**, 5181-5192.
11. B. Logan, *Microbial fuel cells*, John Wiley & Sons, Inc., Hoboken, Jew Jersey, 2008.
12. J. H. Pikul, H. G. Zhang, J. Cho, P. V. Braun and W. P. King, *Nature communications*, 2013, **4**, 1732.
13. H. Ren, H.-S. Lee and J. Chae, *Microfluidics and Nanofluidics*, 2012, **13**, 353-381.
14. Z. L. Wang and J. Song, *Science*, 2006, **312**, 242-246.
15. A. J. Heeger, *Angewandte Chemie International Edition*, 2001, **40**, 2591-2611.
16. D. Pech, M. Brunet, H. Durou, P. Huang, V. Mochalin, Y. Gogotsi, P.-L. Taberna and P. Simon, *Nature nanotechnology*, 2010, **5**, 651-654.
17. H. Ren, S. Pyo, J.-I. Lee, T.-J. Park, F. S. Gittleson, F. C. Leung, J. Kim, A. D. Taylor, H.-S. Lee and J. Chae, *Journal of Power Sources*, 2015, **273**, 823-830.

18. H. Ren, C. I. Torres, P. Parameswaran, B. E. Rittmann and J. Chae, *Biosensors and Bioelectronics*, **61**, 587-592, 2014.
19. J. E. Mink, J. P. Rojas, B. E. Logan and M. M. Hussain, *Nano Lett*, 2012, **12**, 791-795.
20. S. Inoue, *Sensors and Actuators A-Physical*, 2012, **177**, 7.
21. S. Choi, H. S. Lee, Y. Yang, P. Parameswaran, C. I. Torres, B. E. Rittmann and J. Chae, *Lab on a Chip*, 2011, **11**, 1110-1117.
22. Y. Fan, H. Hu and H. Liu, *Journal of Power Sources*, 2007, **171**, 348-354.
23. C. P. B. Siu and M. Chiao, *Microelectromechanical Systems, Journal of*, 2008, **17**, 1329-1341.
24. Y. Fan, S.-K. Han and H. Liu, *Energy & Environmental Science*, 2012, **5**, 8273-8280.
25. A. Dekker, A. T. Heijne, M. Saakes, H. V. Hamelers and C. J. Buisman, *Environmental science & technology*, 2009, **43**, 9038-9042.
26. H. Liu and B. E. Logan, *Environmental Science & Technology*, 2004, **38**, 4040-4046.
27. K. Rabaey, N. Boon, S. D. Siciliano, M. Verhaege and W. Verstraete, *Applied and Environmental Microbiology*, 2004, **70**, 5373-5382.
28. Z. He, S. D. Minteer and L. T. Angenent, *Environmental Science & Technology*, 2005, **39**, 5262-5267.
29. M. Rosenbaum, F. Zhao, U. Schroder and F. Scholz, *Angew Chem Int Edit*, 2006, **45**, 6658-6661.
30. B. R. Ringeisen, E. Henderson, P. K. Wu, J. Pietron, R. Ray, B. Little, J. C. Biffinger and J. M. Jones-Meehan, *Environmental Science & Technology*, 2006, **40**, 2629-2634.
31. J. E. Mink and M. M. Hussain, *ACS nano*, 2013, **7**, 6921-6927.
32. N. S. Malvankar, M. T. Tuominen and D. R. Lovley, *Energy & Environmental Science*, 2012, **5**, 5790-5797.
33. D. R. Bond, S. M. Strycharz-Glaven, L. M. Tender and C. I. Torres, *ChemSusChem*, 2012, **5**, 1099-1105.
34. Y. Liu and D. R. Bond, *ChemSusChem*, 2012, **5**, 1047-1053.
35. S. M. Strycharz-Glaven and L. M. Tender, *ChemSusChem*, 2012, **5**, 1106-1118.
36. X. Xie, L. Hu, M. Pasta, G. F. Wells, D. Kong, C. S. Criddle and Y. Cui, *Nano letters*, 2010, **11**, 291-296.
37. G. Gnana kumar, C. J. Kirubaharan, S. Udhayakumar, K. Ramachandran, C. Karthikeyan, R. Renganathan and K. S. Nahm, *ACS Sustainable Chemistry & Engineering*, 2014, **2**, 2283-2290.
38. Z. He, J. Liu, Y. Qiao, C. M. Li and T. T. Y. Tan, *Nano letters*, 2012, **12**, 4738-4741.
39. H.-T. Chou, H.-J. Lee, C.-Y. Lee, N.-H. Tai and H.-Y. Chang, *Bioresource Technol*, 2014, **169**, 532-536.
40. Y. Qiao, X.-S. Wu, C.-X. Ma, H. He and C. M. Li, *RSC Advances*, 2014, **4**, 21788-21793.
41. Y.-C. Yong, X.-C. Dong, M. B. Chan-Park, H. Song and P. Chen, *ACS nano*, 2012, **6**, 2394-2400.
42. L. Xiao, J. Damien, J. Luo, H. D. Jang, J. Huang and Z. He, *Journal of Power Sources*, 2012, **208**, 187-192.
43. Y. Qiao, C. M. Li, S. J. Bao and Q. L. Bao, *Journal of Power Sources*, 2007, **170**, 79-84.
44. X.-W. Liu, X.-F. Sun, Y.-X. Huang, G.-P. Sheng, S.-G. Wang and H.-Q. Yu, *Energy & Environmental Science*, 2011, **4**, 1422-1427.
45. X. Xie, G. Yu, N. Liu, Z. Bao, C. S. Criddle and Y. Cui, *Energy & Environmental Science*, 2012, **5**, 6862-6866.

46. H. Wang, G. Wang, Y. Ling, F. Qian, Y. Song, X. Lu, S. Chen, Y. Tong and Y. Li, *Nanoscale*, 2013, **5**, 10283-10290.
47. C. I. Torres, A. Kato Marcus and B. E. Rittmann, *Biotechnology and bioengineering*, 2008, **100**, 872-881.
48. A. E. Franks, K. P. Nevin, H. Jia, M. Izallalen, T. L. Woodard and D. R. Lovley, *Energy & Environmental Science*, 2009, **2**, 113-119.
49. Z. Chen, W. Ren, L. Gao, B. Liu, S. Pei and H.-M. Cheng, *Nature materials*, 2011, **10**, 424-428.
50. W. Li, C. Tan, M. A. Lowe, H. D. Abruna and D. C. Ralph, *ACS nano*, 2011, **5**, 2264-2270.
51. P. S. Bonanni, D. F. Bradley, G. D. Schrott and J. P. Busalmen, *ChemSusChem*, 2013, **6**, 711-720.
52. C. I. Torres, A. Kato Marcus and B. E. Rittmann, *Biotechnology and Bioengineering*, 2008, **100**, 872-881.
53. F. Qian, M. Baum, Q. Gu and D. E. Morse, *Lab on a Chip*, 2009, **9**, 3076-3081.
54. J. C. Biffinger, R. Ray, B. Little and B. R. Ringeisen, *Environmental Science & Technology*, 2007, **41**, 1444-1449.
55. X. Jiang, J. Hu, E. R. Petersen, L. A. Fitzgerald, C. S. Jackan, A. M. Lieber, B. R. Ringeisen, C. M. Lieber and J. C. Biffinger, *Nature communications*, 2013, **4**, 2751.
56. X. Jiang, J. Hu, A. M. Lieber, C. S. Jackan, J. C. Biffinger, L. A. Fitzgerald, B. R. Ringeisen and C. M. Lieber, *Nano letters*, 2014, **14**, 6737-6742.
57. D. R. Lovley, *Current opinion in Biotechnology*, 2008, **19**, 564-571.
58. S. J. Roundy, Ph. D Thesis, University of California, 2003.
59. R. Vullers, R. van Schaijk, I. Doms, C. Van Hoof and R. Mertens, *Solid-State Electronics*, 2009, **53**, 684-693.
60. M. Seok, S. Hanson, Y. S. Lin, Z. Foo, D. Kim, Y. Lee, N. Liu, D. Sylvester and D. Blaauw, The Phoenix Processor: A 30pW platform for sensor applications, 2008.
61. M. Hempstead, N. Tripathi, P. Mauro, G. Y. Wei and D. Brooks, An ultra low power system architecture for sensor network applications, 2005.
62. V. Pillai, H. Heinrich, D. Dieska, P. V. Nikitin, R. Martinez and K. V. S. Rao, *Circuits and Systems I: Regular Papers, IEEE Transactions on*, 2007, **54**, 1500-1512.
63. R. Muller, S. Gambini and J. M. Rabaey, *Solid-State Circuits, IEEE Journal of*, 2012, **47**, 232-243.
64. P. Aelterman, K. Rabaey, H. T. Pham, N. Boon and W. Verstraete, *Environmental science & technology*, 2006, **40**, 3388-3394.
65. P. Ledezma, A. Stinchcombe, J. Greenman and I. Ieropoulos, *Physical Chemistry Chemical Physics*, 2013, **15**, 2278-2281.

Figures and captions

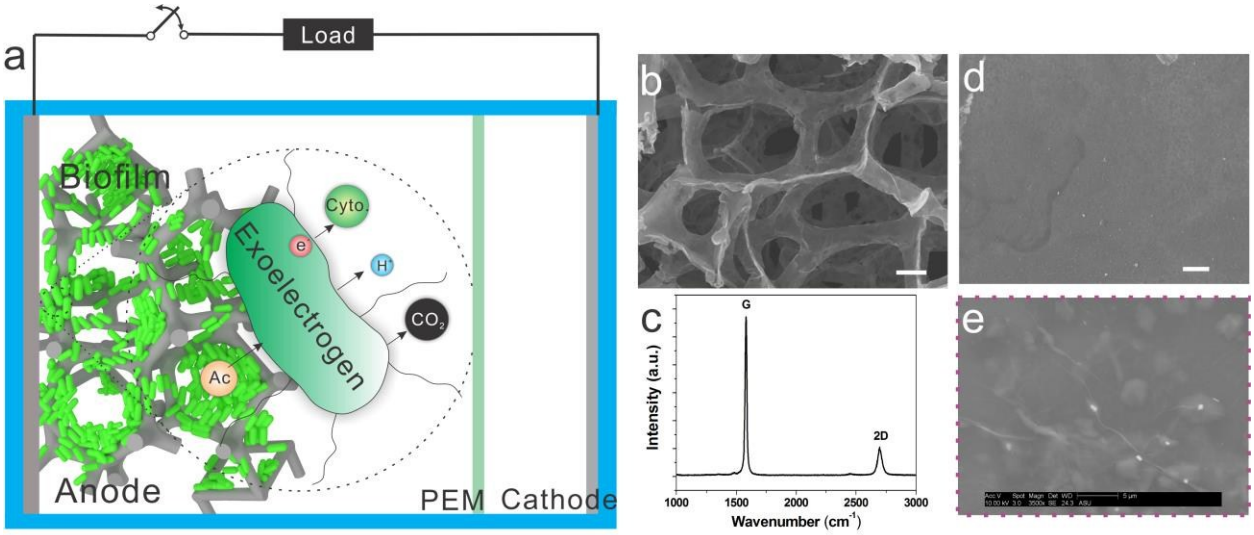

Fig. 1 Schematic of the miniaturized MFC and characterization of different anode materials implemented in the miniaturized MFC: (a) Schematic of the miniaturized MFC having 3D graphene macroporous scaffold anode. The high specific area and macroporosity of the 3D anode allows the growth of larger quantity of biofilm; (b) SEM image of the 3D graphene macroporous scaffold; the 3D free-standing graphene scaffold was fabricated by chemical vapor deposition (CVD) on a nickel template, which was subsequently etched to form a free-standing 3D macroporous graphene scaffold; (c) typical Raman spectra of 3D scaffold; (d) SEM image of the single layer graphene (scale bar: 50μm; (e) is the zoomed-in view of (d)).

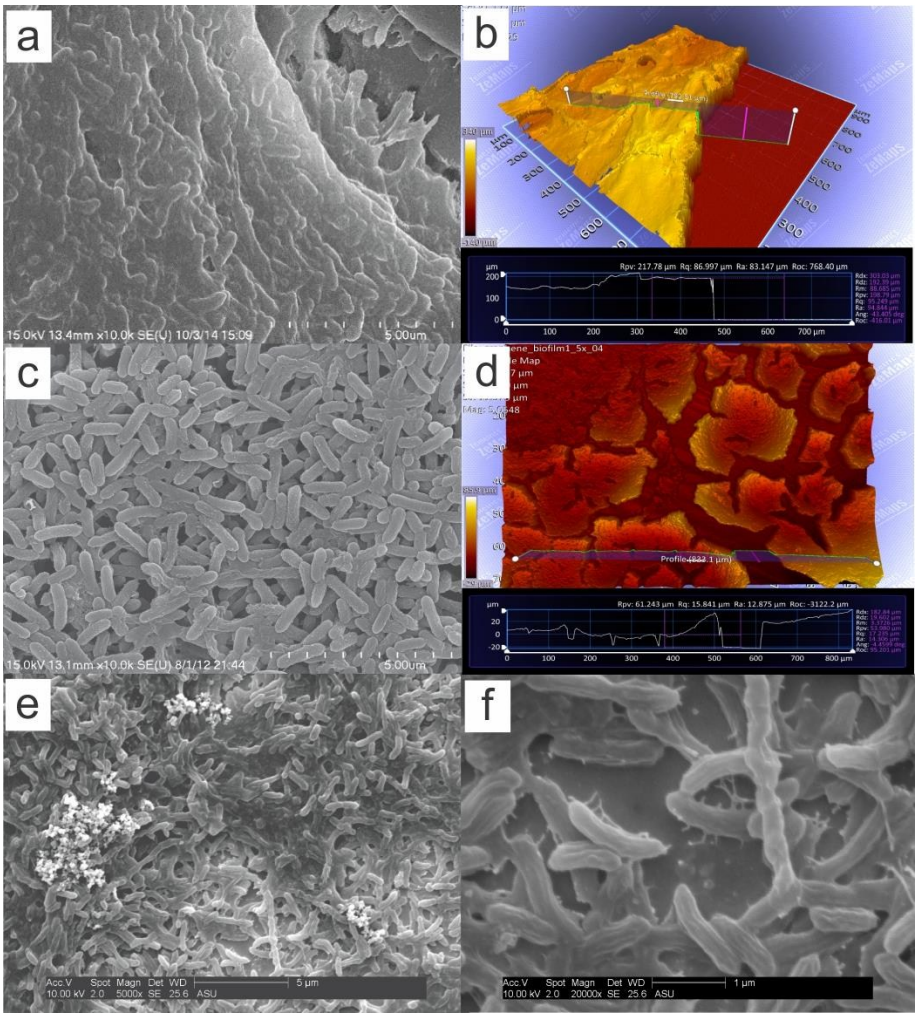

Fig. 2 Morphology of biofilm on anodes imaged by SEM and optical profilometer: (a, b) 3D graphene macroporous scaffold; (c, d) 2D single layer graphene; (e, f) control - bare gold current collector; the biofilm formation on the 3D scaffolds showed a thick and dense biofilm, ~ 150-200 μm thick and 1.6×10^{11} *Geobacter sulfurreducens* / cm^2, on the 3D scaffolds (a, b), matching well with the highest current and power density results found in this study. The biofilm thickness is a total of 5-6 stacks of graphene scaffolds. The biofilm on the 2D single layer graphene (c, d) had a ~ 20-40 μm thick biofilm, which delivered the highest current and power density recorded among planar 2D anodes. The biofilm on the control was approximately 2-3 μm (e, f), only several layers of exoelectrogen were present.

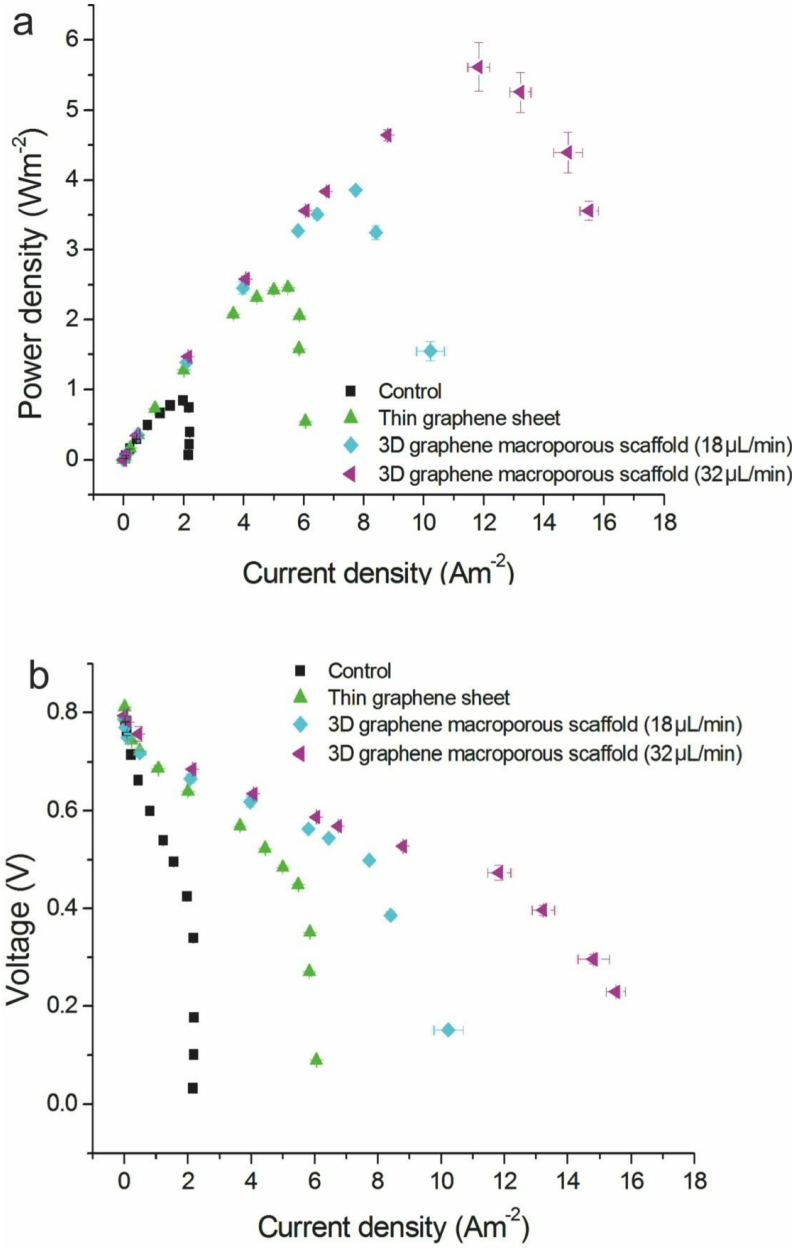

Fig. 3 Polarization curves of the MFCs with different anodes: control, 2D single layer graphene, and 3D graphene macroporous scaffold; all data are collected at 18µL/min, unless specified. The 3D scaffold demonstrated substantially higher current and power density of 15.51 ± 0.30 Am^{-2} and 5.61 ± 0.35 Wm^{-2} at a flow rate of 32 µL/min.

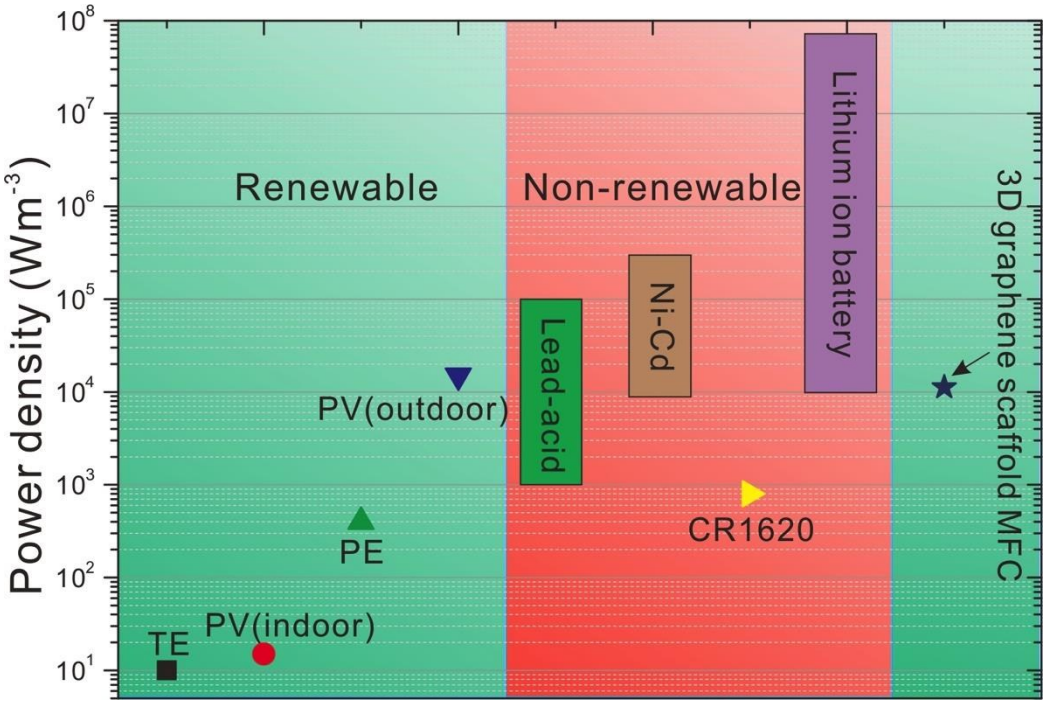

Fig. 4 A comparison of the power density of the MFC with 3D graphene scaffold anode with different power sources and converters, both renewable and non-renewable, including thermoelectricity (TE), piezoelectricity (PE), indoor photovoltaics (indoor PV), outdoor photovoltaics (outdoor PV), lead-acid battery, nickel-cadmium (Ni-Cd) battery, lithium manganese dioxide battery (Sony CR1620) and lithium ion battery. The power density of the MFC with 3D graphene scaffold anode is one to three orders of magnitude higher than TE, PE, PV(indoor) and lithium manganese dioxide battery (Sony CR1620), and comparable with PV(outdoor), lead-acid battery, Ni-Cd battery and lithium ion battery.

Table. 1 Internal resistance and areal resistivity of MFCs with different anode materials and configurations

Electrode	Sheet resistance [Ω/square]	Internal resistance [Ω]	Areal resistivity [Ω·cm^2]
Control	3.65	1625 ± 83	1625 ± 83
Single layer graphene	4.13	487 ± 16	487 ± 16
3D graphene on CC	0.335	219 ± 10	219 ± 10

Table 2. A comparison of specifications of this work compared with prior art.

	Mink et al. [19]	**Inoue et al. [20]**	**Qian et al. [53]**	**Siu et al. [23]**	**Biffinger et al. [54]**	**Ren et al.[17]**	**This work**	
Anode material	CNT	CNT	Gold	Gold	Carbon/Pt ink	CNT	2D single layer graphene	3D graphene
Chamber volume [μL]	1.5	40	1.5	15	25	25	25	50
Anode area [cm^2]	0.25	0.24	0.15	1.2	0.45	0.5	1	1
Inoculum	mixed bacterial culture	Geobacter sulfurreducens	Shewanella putrefacien	Saccharomyces -cerevisiae	Shewanella oneidensis DSP10	Geobacter enriched culture	Geobacter enriched culture	
Substrate	Acetate	Acetate	Lactate	Glucose	LB broth	Acetate	Acetate	
Biofilm thickness (μm)	NA	NA	NA	NA	NA	10	20-40	150-200
Biofilm density (#/cm^2)	NA	NA	NA	NA	NA	0.9×10^{10}	2.8×10^{10}	1.6×10^{11}
Internal resistance [kΩ]	NA	NA	30	25	7.5	2.4	0.487	0.219
Areal resistivity [kΩ·cm^2]	N/A	N/A	4.5	30	3.375	1.2	0.487	0.219
I_{areal} *[A/m^2]*	0.197	0.168	0.13	0.302	0.08	2.59	6.06	15.51
$I_{volumetric}$ *[A/m^3]*	3,947	840	1,300	302	13.3	10,360	24,240	31,020
P_{areal} *[W/m^2]*	0.0196	0.0738	0.015	0.00424	0.06	0.83	2.46	5.61
$P_{volumetric}$ *[W/m^3]*	392	369	15.3	4.24	10	3320	9,820	11,220